The structural, mechanical, electronic, and thermodynamic properties of Cu-doped SnTe studied by first-principles calculations

Q. N. Gao [a], H. L. Zhang [a], Z. H. Dong [a], Y. J. Liu [b], N. N. Zhou [a], P. P. Zhang [a], J. Wang [c,*]

[a] *Department of Mathematics and Physics, Hebei Petroleum University of Technology, Chengde, Hebei, 067500, PR China*
[b] *Department of Admission and Employment, Hebei Petroleum University of Technology, Chengde, Hebei, 067500, PR China*
[c] *State Key Laboratory of Powder Metallurgy, Central South University, Changsha, Hunan 410083, PR China*

The structural, mechanical, electronic, and thermodynamic properties of $Cu_xSn_{1-x}Te$ ($x = 0$, 0.03125, 0.0625, 0.125, and 0.25) are investigated through first-principles calculations. The studied structures are all cubic and own negative enthalpy of formation. The elastic constants and mechanical properties (B, G, E and v) are predicted. The bandgap of SnTe evaluated by HSE06 is 0.25 eV, closing to the experimental data 0.19 eV. All studied Cu-doped compounds behave metallic. In addition, the thermodynamic properties (G, H, S, C_P, and C_V) of the materials, together with the bulk modulus and thermal expansion coefficient versus temperature have been evaluated.

1. Introduction

Te-based chalcogenide is a vital material in Phase Change Random Access Memory (PCRAM) area, which have got much notice [1, 2]. Among Te-based materials, tin telluride is a candidate of thermoelectric material suitable for mid-temperature usage, attracting considerable attention from researchers because of its promising uses in waste heat recovery, cooling systems, and power generation [3-6]. Recent studies have concentrated on Te-based compounds especially doping SnTe with different elements to enhance its thermoelectric properties [7-10]. Such as the investigations of structure, mechanical, thermoelectric and optical properties on SnTe doped with Se element, SnTe doped with Bi and Se element by Muthumari et al. [9, 11], Zn–Mn co-doped SnTe by Bugalia et al. [7], topological insulator SnTe-class materials by Wang et al. [8], Mn-doped SnTe by Liu et al. [10], Ag-Cu co-doped SnTe by Jamwal et al. [12] and so on. As report, dilute concentration of co-doped Ag-Cu could increase the bandgap of SnTe and improve the thermoelectric properties as well.

However, there is no investigation of SnTe with Cu. Therefore, this study primarily focuses on the characteristics of Cu-doped SnTe materials. According to the report about the influence of strain on the bandgap of SnTe [13] under certain conditions, it can be concluded that investigations into the strain-dependent elastic properties are beneficial for designing materials [14], the elastic constants are highly valuable for supporting the impact of strain in different directions of a material [15, 16]. Based on the reviews above, it is found that the study of elastic parameters from both experimental and theoretical perspectives is not as extensive. Especially, the research on the mechanical properties of SnTe doped with some elements is even more lacking. Consequently, it is imperative to examine the mechanical properties, including elastic constants (C_{ij}), shear modulus (G), bulk modulus (B), Young's modulus (E), and Poisson's ratio (v), of Cu-doped SnTe materials. The optimization of synthesis and crystal growth conditions for materials is critically dependent on the realization of their thermodynamic functions [17]. Thermal expansion is a critical physical property that, in certain instances, determines the feasibility of a material's practical application and through doping this parameter generally increases [18]. The conclusion is in accordance with the theoretical predications [19, 20], which demonstrated that the configurational entropy of doped materials increasing lead to the increase of α, and α is also related to the heat capacity and Grüneisen parameter which are usually influenced by free charge carriers [17]. High-temperature thermophysical properties: heat capacity, entropy, and enthalpy are key parameters describing the thermophysical properties of materials. For example, heat capacity makes a considerable impact on the stability and efficiency of thermoelectric devices as it affects the material's response and storage capacity for heat. Entropy and enthalpy can help us understand the thermal stability and phase transition behavior of materials at different temperatures. These can be proved by the previous work on Te-X (X = As, Si, Co) compounds [1]. For SnTe, research on these high-temperature thermophysical properties can help us optimize its performance in thermoelectric devices. However, thermodynamic data of SnTe and Cu-doped SnTe is particularly scarce.

Essentially, the mechanical properties and thermodynamic properties of SnTe and Cu-doped SnTe materials are calculated by first-principles method. For the doped SnTe materials, the Sn atoms will be replaced with Cu atoms. Based on the commonly used doping concentrations of semiconductor materials studied in the literature, this work plans to investigate the following compounds: $Cu_{0.03125}Sn_{0.96875}Te$, $Cu_{0.0625}Sn_{0.9375}Te$, $Cu_{0.125}Sn_{0.875}Te$, and $Cu_{0.25}Sn_{0.75}Te$. The aim is to acquire a more profound insight of the properties of SnTe materials, providing theoretical guidance for further research, preparation, and application of SnTe materials.

2. Methodology

In Section 2.1, the calculation process of elastic constants and mechanical properties is briefly described. Section 2.2 introduces the quasi-harmonic method. The settings of ab initio calculations are detailed in Section 2.3.

2.1. The calculation progress of mechanical properties

With the view of estimating the mechanical properties of Cu-doped SnTe materials, the strain–stress method in vaspkit procedure[21], are adopted. Hooke's law states that the strain as a function of stress is expressed as $\sigma=\varepsilon c$, in which c represents the elastic stiffness constants,

forming a 6×6 matrix. For rocksalt crystals, there just exist three independent elastic constants C_{11}, C_{12}, and C_{44}. For cubic system, C_{11} and C_{12} are associated with longitudinal compression and transverse expansion, respectively. Meanwhile, C_{44} is linked to the shearing deformation of the crystal.

Under the strain-stress method in vaspkit procedure, 7 deformations around the equilibrium volume of each structure have been adopted.

Once the elastic stiffness constants have been obtained, the elastic properties of targeted materials containing B, G, E, and v can be predicted on the basis of two methods put forward by Voigt [22] and Reuss [23] separately.

2.2 The quasi-harmonic approach

In current work, the quasi-harmonic approach is utilized to calculate the thermodynamic properties of $Cu_xSn_{1-x}Te$ (x = 0, 0.03125, 0.0625, 0.125, and 0.25). On the basis of the method, the Helmholtz free energy $F(V,T)$ as a function of volume V and temperature T is usually expressed as follows [24]

$$F(V,T)=E_c(V)+F_{ele}(V,T)+F_{vib}(V,T) \tag{1}$$

In this equation, the term $E_c(V)$ represents the static energy at 0 K, which is calculated from energy-volume curves. These curves are then fitted using a four-parameter Birch–Murnaghan equation of state [24]

$$E_c(V)=a+bV^{-2/3}+cV^{-4/3}+dV^{-2} \tag{2}$$

In equation (2), a, b, c, and d are fitting parameters. The equation of states (EOS) yields equilibrium parameters including volume (V_0), energy (E_0), bulk modulus (B), and its first pressure derivative (B'). The second component of Eq. (1), $F_{ele}(V,T)$ denotes the component of thermal electronic contribution to Helmholtz free energy, calculated using Mermin statistics [24]. The third term, $F_{vib}(V,T)$, denotes the contribution of vibration to Helmholtz free energy, estimated in this study using the Debye-Grüneisen model [25]. According to the Debye-Grüneisen model, Θ_D is expressed as

$$\Theta_D=sAV_0^{1/6}(\frac{B_0}{M})^{1/2}(\frac{V_0}{V})^{\gamma} \tag{3}$$

In equation (3), the scaling factor s is equal to 0.617 for nonmagnetic cubic phases, which is evaluated by Moruzzi et al. [26]. M is the atomic mass, γ the Grüneisen parameter expressed as $\gamma=[\frac{1+B_0'}{2} - x]$. For investigations of high temperature situation, x in γ is usually set to 2/3, and for low temperature situation x equal to 1 . The parameter A is a constant, which is expressed as $A=(6\pi^2)^{1/3} \hbar/k_B =231.04$ with V in Å^3, B in GPa, and M in atomic mass of gram.

Utilizing Eq. (1), it is possible to calculate the Helmholtz free energies for $Cu_xSn_{1-x}Te$ (x = 0, 0.03125, 0.0625, 0.125, and 0.25). Once the Helmholtz free energy is determined, various thermodynamic properties can be derived, including entropy (S), enthalpy (H), and heat capacity at constant volume/pressure (C_V/C_P). These properties are obtained through the application of specific equations:

$$S=-(\frac{\partial F}{\partial T})_V \tag{4}$$

$$H=F+TS \tag{5}$$

$$C_V=-T\left(\frac{\partial S}{\partial T}\right)_V \tag{6}$$

$$C_P=C_V^{\text{ele}}+C_V^{\text{vib}}+\alpha^2 B_T T V_T \tag{7}$$

In equation (7), C_V^{ele} represents the thermal electronic component of heat capacity, C_V^{vib} denotes the vibrational component of heat capacity, α signifies the thermal expansion coefficient of materials, B_T indicates the isothermal bulk modulus, and V_T stands for the equilibrium volume at the considered temperature in present work.

2.3. Settings of calculation process

In current work, the Vienna Ab initio Simulation Package (VASP) [27, 28] is employed for conducting all computations. To model the interactions between electrons and ions, the projector augmented wave (PAW) method [29] is implemented. The exchange-correlation (X-C) functional is handled using the Perdew-Burke-Ernzerhof generalized-gradient approximation (GGA) [30], except that hybrid functionals HSE06 [31] is adopted to evaluate the band structures of the structures studied in present work. The cutoff energy is established at 500eV. For the electronic self-consistency and ionic relaxation loops, the convergence thresholds are set to 10^{-6} eV/atom and 10^{-5} eV/atom, respectively. For structural relaxations, the Gaussian smearing technique [32] is employed, while the final calculations utilize the linear tetrahedron method with Blöchl corrections [33]. The sampling of k-point is conducted adopting the Monkhorst-Pack scheme [34].

The known crystal structure of SnTe is rocksalt [35], owning eight atoms, as displayed in Fig.1. In order to dope impurity elements, we construct a $3\times3\times3$ supercell containing 64 atoms for making Cu doped SnTe materials. We replace Sn with one, two, four and eight Cu atoms and get $Cu_xSn_{1-x}Te$ (x = 0.03125, 0.0625, 0.125, 0.25) compounds. All structures studied here are fully relaxed with k-points set to $5\times5\times5$.
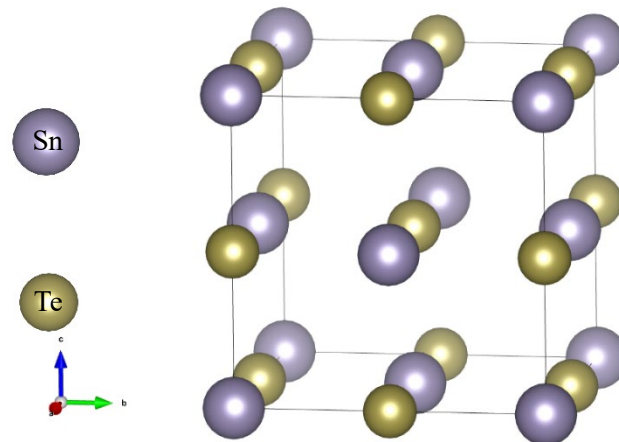
Fig.1. The unit cell structure of SnTe.

3. Results and discussions

3.1. Ground state properties

The rocksalt structure SnTe belongs to Fm-3m space group with the number 225. The ground state properties of $Cu_xSn_{1-x}Te$ ($x = 0$, 0.03125, 0.0625, 0.125, 0.25) materials can be deduced by Birch-Murnaghan equation, expressed as equation (2) [24]. These properties include V_0, E_0, B_0 and B', which are listed in Tabel 1. The E-V curves of different structures are plotted in Fig. 2, which can indicate the stability of the targeted materials.
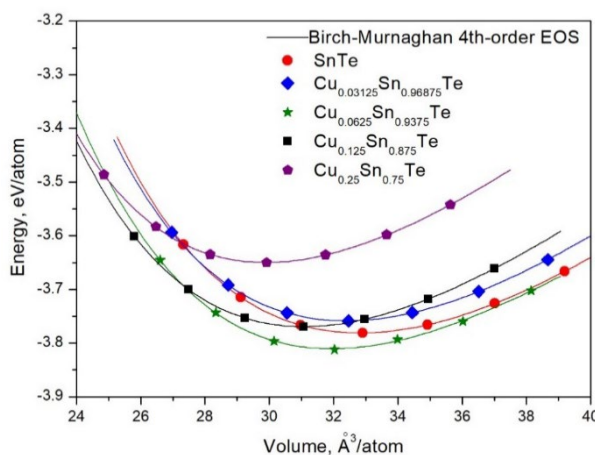
Fig. 2. The E-V curves of $Cu_xSn_{1-x}Te$ (x = 0, 0.03125, 0.0625, 0.125, 0.25) materials.

As seen in Table 1, the present predicted lattice constant a of SnTe is larger than the reported measured data [36, 37] merely 1.18% and consistent with the available calculated ones in literature [38, 39]. The bulk modulus (B_0) is 4.7% lager than the datum measured by Okoye [39]. The other calculated bulk modulus lies between 37.0 to 44.5 Gpa [38-40]. There is an article reviewed by Lejaeghere et al. [41] reporting that the data of volume and B_0 obtained by GGA exist 3.8% and 4.7% systematic deviation, respectively. The estimated residual error margins resulting from algorithmic variations and numerical errors in B_0 are approximately 15 GPa. Considering this, our findings demonstrate excellent concordance with experimental observations.

At various concentration of Cu doped SnTe materials, to determine the energetically favorable configuration, structural optimization is conducted. Additionally, the enthalpy of formation (ΔH) is calculated to assess the thermodynamic stability of $Cu_xSn_{1-x}Te$ ($x = 0$, 0.03125, 0.0625, 0.125, 0.25) compound, which is expressed as [42]:

$$\Delta H = E_{total}(Cu_xSn_{1-x}Te) - xE(Cu) - (1-x)E(Sn) - E(Te) \tag{8}$$

Here, $E_{total}(Cu_xSn_{1-x}Te)$, $E(Cu)$, $E(Sn)$ and $E(Te)$ are the minimum energy of $Cu_xSn_{1-x}Te$, fcc Cu, diamond Sn and trigonal Te, respectively. x is the mole fraction of Cu atom. The evaluated formation enthalpies are negative revealing the stability of the Cu doped SnTe materials, as seen in Table 1.

Table 1. The lattice constant a, space group, structure, ΔH, B_0,
and B' of $Cu_xSn_{1-x}Te$ (x = 0, 0.03125, 0.0625, 0.125, 0.25) materials.

		$a(\text{Å})$	Space group	Structure	$\Delta H(\text{eV})$	$B_0(\text{GPa})$	B'
SnTe	PW	6.403	225 Fm-3m	Cubic	-13.19	40.2	4.3
	Expt.	6.328[a]				38.4[a]	
	Calc.	6.318[b] 6.404[c] 6.230[d] 6.405[e]				40.1[c] 37.0[d] 44.5[e]	4.3[c] 3.57[e]
$Cu_{0.03125}Sn_{0.96875}Te$	PW	6.383	221 Pm-3m	Cubic	-12.04	40.8	4.3
$Cu_{0.0625}Sn_{0.9375}Te$	PW	6.352	229 Im-3m	Cubic	-15.72	41.4	4.5
$Cu_{0.125}Sn_{0.875}Te$	PW	6.288	225 Fm-3m	Cubic	-13.26	42.6	4.6
$Cu_{0.25}Sn_{0.75}Te$	PW	6.206	221 Pm-3m	Cubic	-6.91	43.6	4.7

PW: Present work

[a] [36]

[b] [37]

[c] [39]

[d] [40]

[e] [38]

3.2. Mechanical properties

Tables 2 and 3 present the compiled data for the $Cu_xSn_{1-x}Te$ compounds (where $x = 0$, 0.03125, 0.0625, 0.125, 0.25), including their elastic constants and elastic properties. The elastic properties encompass B, G, E, and v. The elastic constants C_{ij} of SnTe studied in the present work show good consistency with the data measured by Every et al. [43] and Madelung et al. [36]. Meanwhile, the present results are also in accordance with the calculated ones by Kumar et al. [38].

For a rocksalt structure, the indispensable and efficient Born stability criterion are prescribed by Mouhat and Coudert [44], which is as follows:

$$(C_{11}-C_{12})>0, \ (C_{11}+2C_{12})>0, \ C_{44}>0 \tag{9}$$

On the basis of equation (9) and the elastic constants of $Cu_xSn_{1-x}Te$ ($x = 0$, 0.03125, 0.0625, 0.125, 0.25) listed in Table 2, it is easy to find all compounds fit the Born stability criterion. Hence, the structures studied here are all mechanically stable. Based on the calculated elastic constant, the anisotropy $A = 2C_{44}/(C_{11}-C_{12})$ prescribed by Chattopadhyay et al.[45] is evaluated and listed in Table 2 as well. The anisotropy of the targeted compounds less than 1 indicate rigidity along the [100] direction.

Table 3 presents additional mechanical properties derived from the elastic constants, along with previously reported results. The current findings show excellent consistency with both reported measured data [36] and other predicted ones [38]. Notably, the mean bulk modulus B_H is comparable to the value obtained by the *E-V* data. The slight difference may be attributed to the strain-stress method, in which the strains apply in various directions.

Elastic constants provide insights into the tendencies of materials regarding vacancy formation, movement, and diffusion sensitivity. This knowledge has practical applications in manufacturing processes that involve annealing and deformation. The formula for calculating the enthalpy of vacancy migration H_M is as follows [46]:

$$H_M = \delta^2 G_F a^3 \tag{10}$$

where $G_F = \dfrac{15C_{11}C_{44}B}{2[3C_{44}B+C_{11}(2C_{44}+B)]}$, $B=(C_{11}-C_{12})$ and $\delta^2=0.22$ for rocksalt crystals. For SnTe, the result calculated based on the above formula is 2.404eV. This datum is consistent with the one predicted by Kumar et al. [38]. Based on high-throughput calculations, Angesten et al. [47] proposed another relationship as follows:

$$H_M=0.016B_0 a^3 \tag{11}$$

The H_M of SnTe calculated by Eq. (11) is 1.057eV, showing a semblable result with that of Kumar et al. [38]. The H_M of other compounds investigated through the above two methods are collected in Table 2.

Table 2. The elastic constants C_{ij} of SnTe.

		C_{ij}(Gpa)			A	H_M(eV)	
		C_{11}	C_{12}	C_{44}			
SnTe	PW	111.3	3.5	14.9	0.28	2.404	1.057
	Expt.	109.3[a]	2.1[a]	9.7[a]			
		118.0[f]	4.1[f]	14.5[f]			
	Calc.	116.7[e]	3.7[e]	15.2[e]			2.477	1.17
$Cu_{0.03125}Sn_{0.96875}Te$	PW	98.0	8.2	15.0	0.33	2.243	1.061
$Cu_{0.0625}Sn_{0.9375}Te$	PW	99.6	12.3	13.7	0.31	2.097	1.061
$Cu_{0.125}Sn_{0.875}Te$	PW	88.9	19.2	12.8	0.37	1.824	1.059
$Cu_{0.25}Sn_{0.75}Te$	PW	111.7	10.0	12.9	0.25	2.023	1.042

[a] [43]

[f] [36]

[e] [38]

Table 3. The predicted B, G, E and v of SnTe evaluated by Voigt, Reuss, and Hill approximations. The data of G, E and v are distinguished by V, R and H, respectively.

			G(Gpa)			E(Gpa)			v		
		B_H	G_V	G_R	G_H	E_V	E_R	E_H	v_V	v_R	v_H
SnTe	PW	39.4	30.6	21.0	25.8	72.8	53.6	63.5	0.190	0.273	0.231
	Expt.[43]	38.4									
	Calc.[38]	41.4	31.7	21.5	26.6	75.8	54.9	65.4	0.195	0.278	0.228
$Cu_{0.03125}Sn_{0.96875}Te$	PW	38.2	27.0	20.5	23.7	65.6	52.2	59.0	0.210	0.272	0.242
$Cu_{0.0625}Sn_{0.9375}Te$	PW	41.4	25.7	18.9	22.3	63.8	49.1	56.6	0.240	0.302	0.272
$Cu_{0.125}Sn_{0.875}Te$	PW	42.4	21.6	17.1	19.4	55.4	45.3	50.4	0.280	0.322	0.302
$Cu_{0.25}Sn_{0.75}Te$	PW	43.9	28.1	18.4	23.2	69.4	48.5	59.3	0.240	0.316	0.275

3.3. Electronic properties

The electronic characteristics of a system, for instance, its band structure (BS) and the electrons   distributed in bands, play a crucial role in determining its applications [48]. To elucidate the electronic properties of the $Cu_xSn_{1-x}Te$ (x = 0, 0.03125, 0.0625, 0.125, 0.25) materials, calculations of the band structure and density of states (DOS) are performed within the first Brillion Zone. The parent SnTe material owns direct band gap of 0.06 eV evaluated by PBE functionals. This datum shows good consistency with the other theoretically predicted values 0.05 eV calculated by Kumar et al. [38] and 0.06 eV calculated by Okoye [39], which both use the same PBE functionals. Nevertheless, the data obtained by PBE functionals are lower than the ones of 0.19 eV measured by Kannaujiya et al. [49], 0.11 eV calculated by Tan et al. [50], and 0.14 eV evaluated by Wang et al. [51] and Moshwan et al. [52].

The PBE functions are well-known for consistently underestimating the bandgap. In some cases, hybrid functionals, which combine the exchange component of GGA functional with Hartree-Fock theory's exact exchange, can produce a bandgap value that closely approximates experimental measurements. [53]. Hence, the bandgap of SnTe is predicted by the extensively used hybrid functionals HSE06 [31]. The result of 0.25 eV obtained by this method is very close to the experimental data 0.19 eV, meanwhile it is more reasonable than the 1.30 eV evaluated by Kumar et al. [38] using HSE06. This difference may result from the different pseudopotentials adopted in our works. Kumar et al. [38] have adopted plane-wave pseudopotential (PW-PP) method, while the projector augmented wave (PAW) method has been utilized in the current work.

In addition, the band structures of $Cu_xSn_{1-x}Te$ (x = 0, 0.03125, 0.0625, 0.125, 0.25) are calculated by HSE06 as well, shown in Fig. 3. It is seen that Cu doped SnTe materials $Cu_xSn_{1-x}Te$ (x = 0.03125, 0.0625, 0.125, 0.25) exhibit metallic behavior.
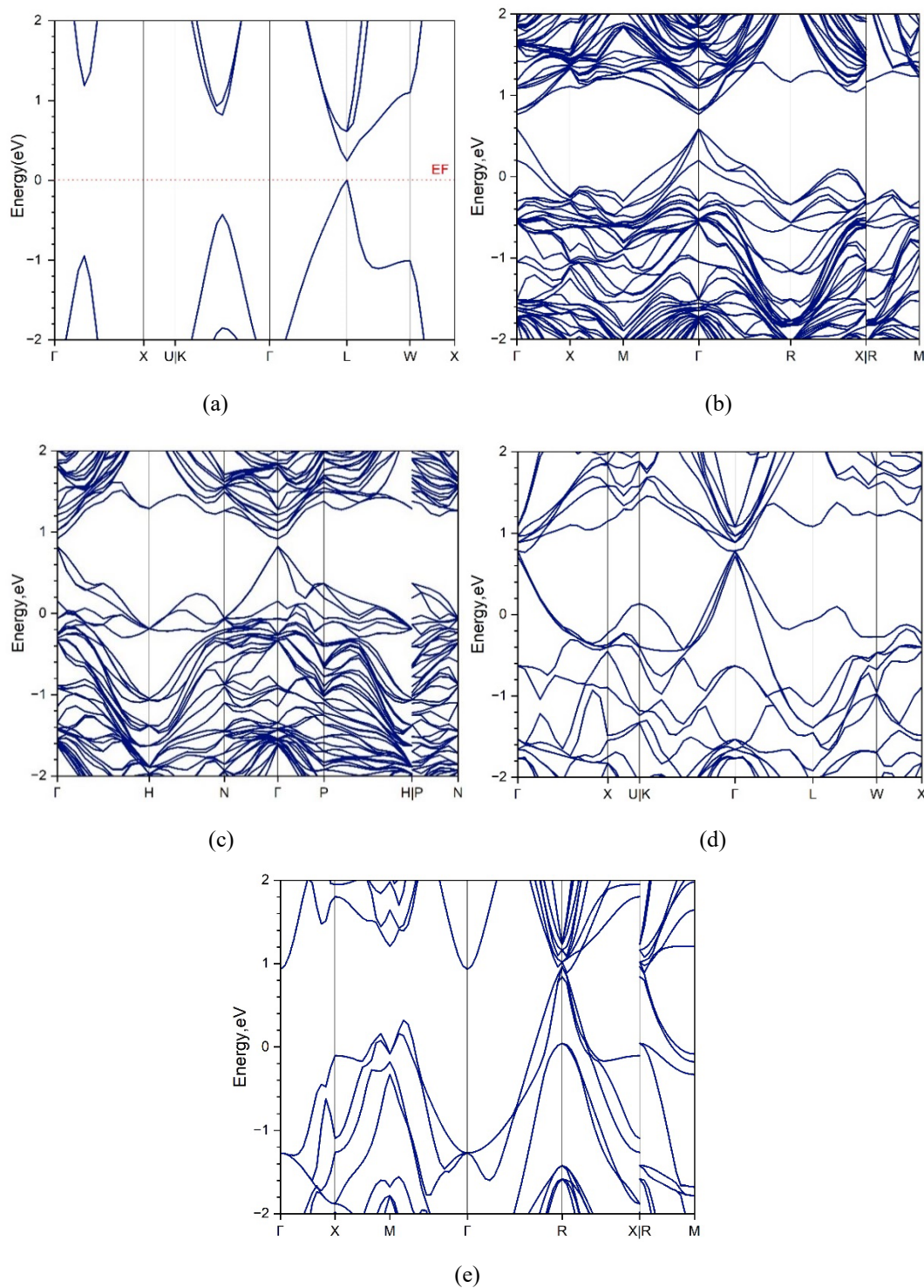
Fig. 3. The band structures of $Cu_xSn_{1-x}Te$ (x = 0, 0.03125, 0.0625, 0.125, 0.25) compounds are displayed in (a), (b), (c), (d) and (e), respectively.

The total and partial density of states (TDOS and PDOS) for Cu doped SnTe materials $Cu_xSn_{1-x}Te$ (x = 0, 0.03125, 0.0625, 0.125, 0.25) are displayed in Fig. 4. As shown in Fig. 4(a), there exists a narrow band at -10.9 eV of the TDOS of SnTe. This narrow band is mostly contributed by the Te-s orbitals, which can be verified by the PDOS of SnTe. Above and adjacent to the Fermi level,

the TDOS is primarily influenced by Sn-p orbitals, whereas Te-p orbitals are the main contributors to the TDOS below the Fermi level. It can be discovered that the first sharp peak of the total DOS lies at -10.6 eV by Te-s states, as seen in Fig. 4(b). The second peak is found at -6.6 eV mostly contributed by Sn-s states and partially by Te-s and Te-p orbitals. Below the Fermi level, the Te-p orbitals still fulfill a crucial function, while Sn-p and Cu-d states are partially contributed. The total DOS cross over the Fermi level is crucial influenced by Te-p and Cu-d orbitals according to the inset in Fig. 4(b). Upon the Fermi level, Sn-p orbital states exert a decisive influence. For the total DOS of $Cu_{0.0625}Sn_{0.09375}Te$ seen in Fig. 4(c), the first peak locates at -10.7 eV due to Te-s states and the second peak locates at -6.9 eV mainly by Sn-s and partially by Te-s and Te-p states. Below the fermi level, there exist another peak, which is mainly influenced by Te-p and Cu-d orbitals.
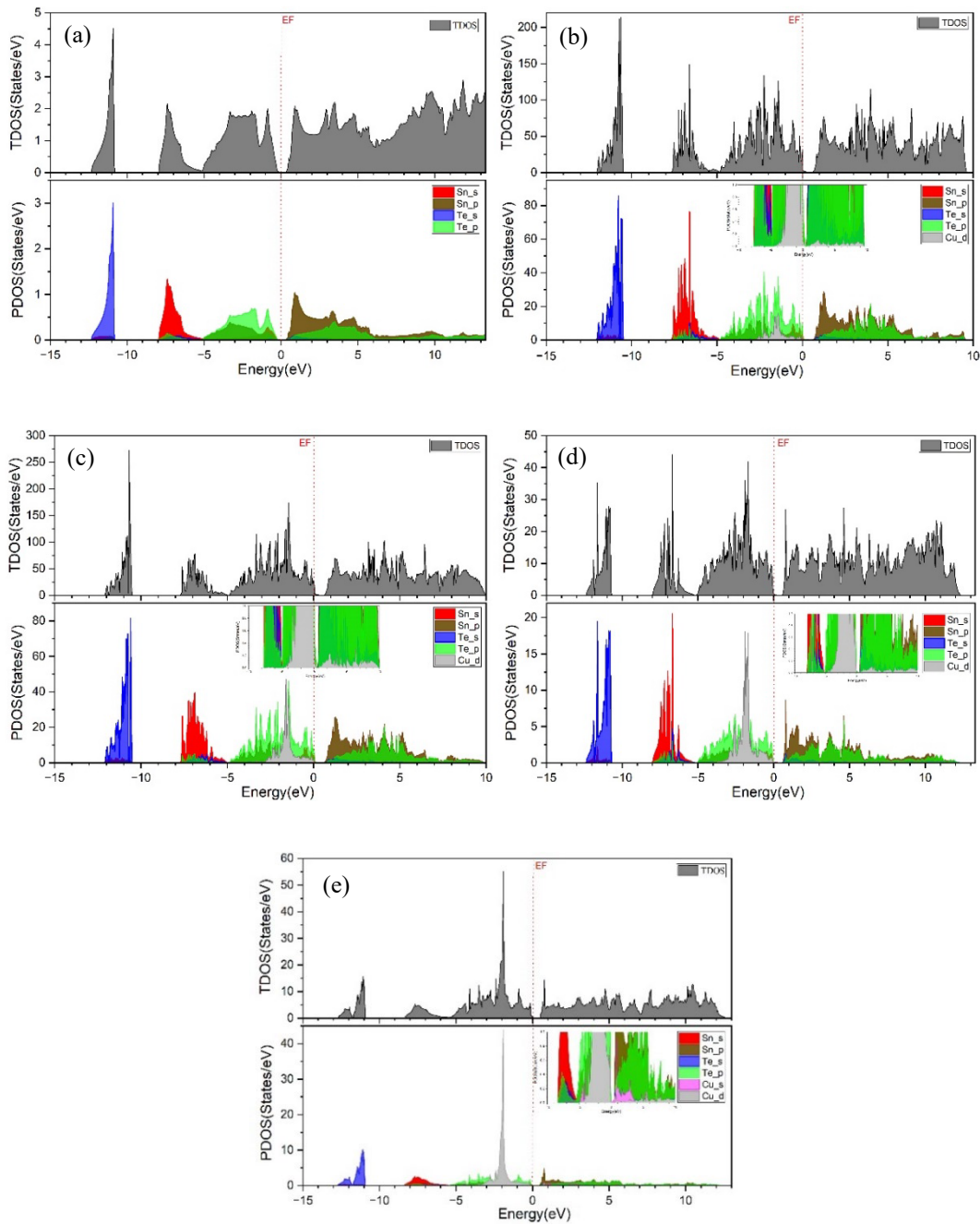
Fig. 4. The TDOS and PDOS of SnTe, $Cu_{0.03125}Sn_{0.96875}Te$, $Cu_{0.0625}Sn_{0.09375}Te$, $Cu_{0.125}Sn_{0.875}Te$, and $Cu_{0.25}Sn_{0.75}Te$ are displayed in (a), (b), (c), (d), and (e), respectively.

It also can be observed that Te-p and Cu-d states cross through Fermi level making the Cu doped material behaves metallic. Upon the Fermi level, the Sn-p and Te-p orbitals play a crucial role. With the increasing content of Cu, the contribution of doped Cu adjacent to Fermi level is more obvious, which is verified in Fig. 4(d) and (e). In Fig. 4(d), a taller and sharper peak appeared at the front of the first peak locating at -11.5 eV deviating from the first peak 0.8 eV mostly due to Te-s states. The second peak is also split into several sharp peaks, with the highest peak located at -6.5 eV due to the influence of Sn-s, Te-s, and Te-p electronic states. The third peak below the Fermi level is at -1.5 eV, mainly contributed by Cu-d electrons. Around and above the Fermi level, the contributions for the metallic behavior come from Sn-p, Te-s, Te-p and Cu-d electrons. As the Cu content increases, the third peak at -1.5 eV caused by the Cu-d electrons becomes much higher than the other peaks, as seen in Fig. 4(e). Near the fermi level, the contributions for metallic is not only from Sn-p, Te-p, Cu-d electrons, but also partially from Cu-s states.

3.4. Thermodynamic properties

On the basis of the current calculated equilibrium properties V_0, E_0, B and B' listed in Table 1 and the electronic state density (EDOSs) which is usually directly predicted through first-principles calculations, the Helmholtz free energies of $Cu_xSn_{1-x}Te$ (x = 0, 0.03125, 0.0625, 0.125, 0.25) materials have been evaluated based on Eq. (1). Given that the computations in the present work are conducted at zero external pressure, the Helmholtz free energy is equivalent to the Gibbs free energy. By incorporating the vibrational and thermal electronic components, the finite-temperature thermodynamic properties (including G, S, H, and C_P) of $Cu_xSn_{1-x}Te$ (x = 0, 0.03125, 0.0625, 0.125, 0.25) materials have been evaluated according to equations (3) - (7), which are displayed in Fig. 5(a)-(e) separately. It is noticeable that the reference state for G and H is H at 298.15 K. For contrast, the CALPHAD assessed results of SnTe conducted by Liu et al. [54] are demonstrated in Fig. 5(a) as well. In Fig. 5(a), it is observed that the predicted enthalpy, entropy and heat capacity agree very well with the thermodynamic modeled results. But for Gibbs energy, a significant difference exists between the current findings and the CALPHAD-modeled results, possibly due to the limited thermodynamic data utilized in CALPHAD modeling. From the calculating data of SnTe, the quasi-harmonic Debye model proves to be an appropriate method suitable for semiconductors. For other compounds $Cu_xSn_{1-x}Te$ (x = 0.03125, 0.0625, 0.125, 0.25) lacking modeled and measured results, the thermodynamic properties are also predicted for further investigations.

Fig. 6 displays the temperature-dependent heat capacity at constant volume of $Cu_xSn_{1-x}Te$ (x = 0, 0.03125, 0.0625, 0.125, 0.25). As seen in Fig. 6, the heat capacity increases sharply as the temperature rises at lower temperature ranges. Meanwhile, in the high-temperature region, C_V approaches the Dulong-Petit limit $3R$ ($\approx$ 24.9 J·mol^{-1}K^{-1}) [55].

According to Eq. (3), the Debye temperatures of $Cu_xSn_{1-x}Te$ (x = 0, 0.03125, 0.0625, 0.125, 0.25) are 146.5 K, 147.6 K, 148.4 K, 150.8 K and 153.7 K, respectively. The datum of SnTn is a little lower than the experimental value 170 K [37]. With the increasing Cu concentration, the Debye temperatures of $Cu_xSn_{1-x}Te$ (x = 0, 0.03125, 0.0625, 0.125, 0.25) increase.
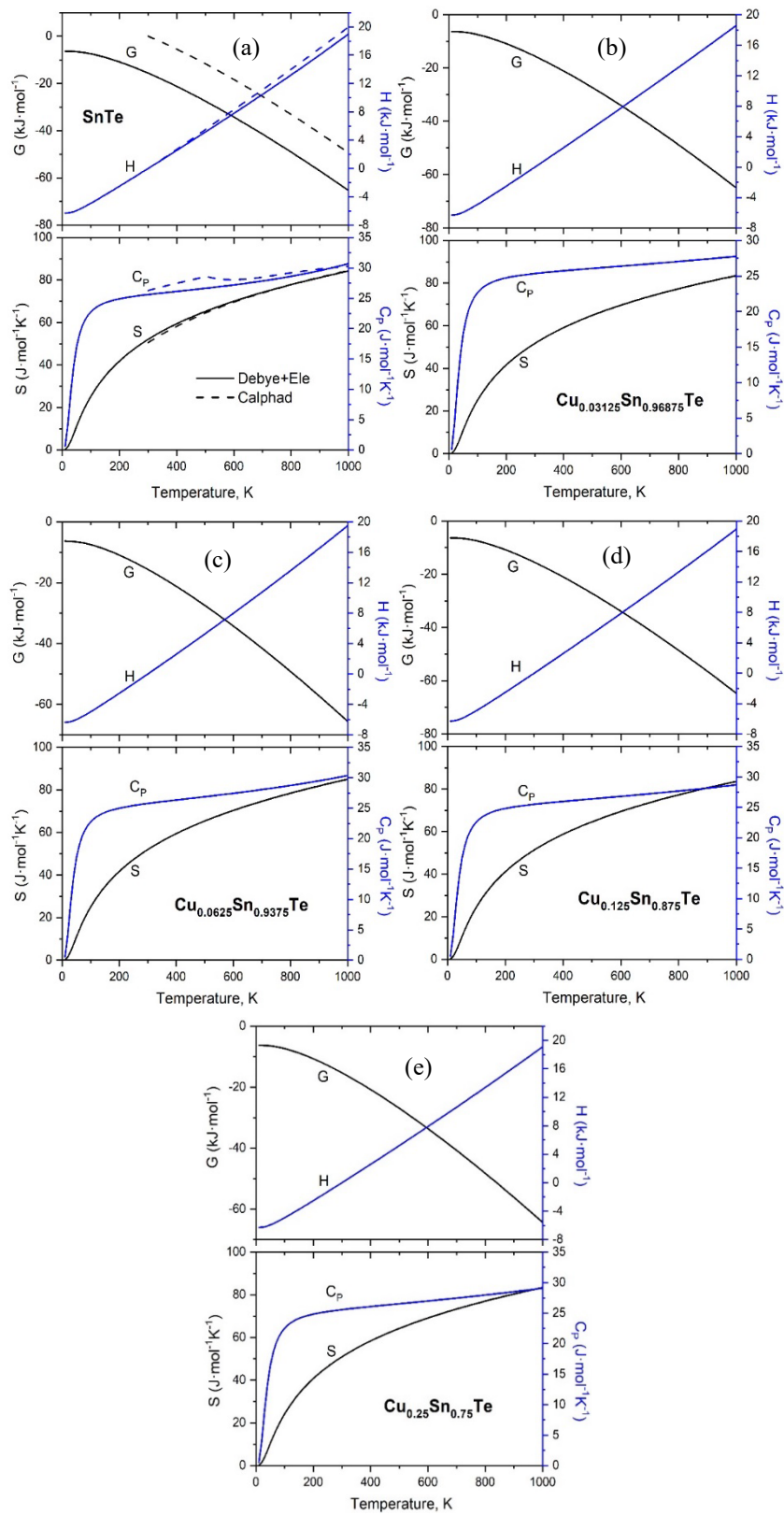
Fig. 5. The predicted thermodynamic properties of Cu$_x$Sn$_{1-x}$Te (x = 0, 0.03125, 0.0625, 0.125, 0.25) are displayed in (a), (b), (c), (d) and (e), respectively. These properties include G, S, H and C$_P$. For contrast, the results of the existing CALPHAD modeling conducted by Liu et al. [54] are presented. The reference state for G and H is H at 298.15 K.
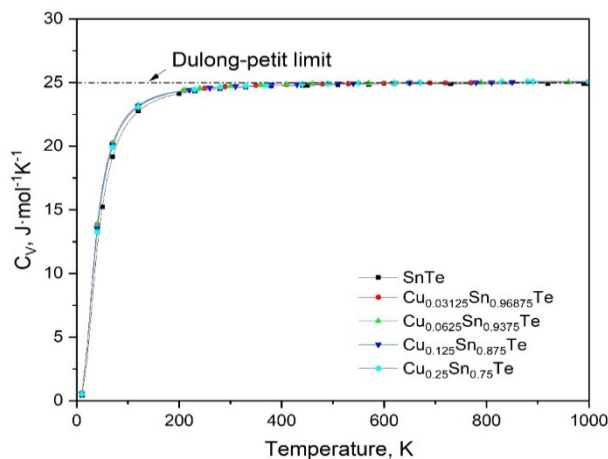
Fig. 6. C_V of $Cu_xSn_{1-x}Te$ (x = 0, 0.03125, 0.0625, 0.125, 0.25) compounds versus temperature.

Coefficient of thermal expansion is an important parameter for the safe operation of thermoelectric devices. The thermal expansion coefficients, together with the bulk modulus of $Cu_xSn_{1-x}Te$ (x = 0, 0.03125, 0.0625, 0.125, 0.25) materials versus temperature are demonstrated in Fig. 7. It is easily to observe that the bulk moduli of the target materials decrease with rising temperature linearly, seen in Fig. 7(a).
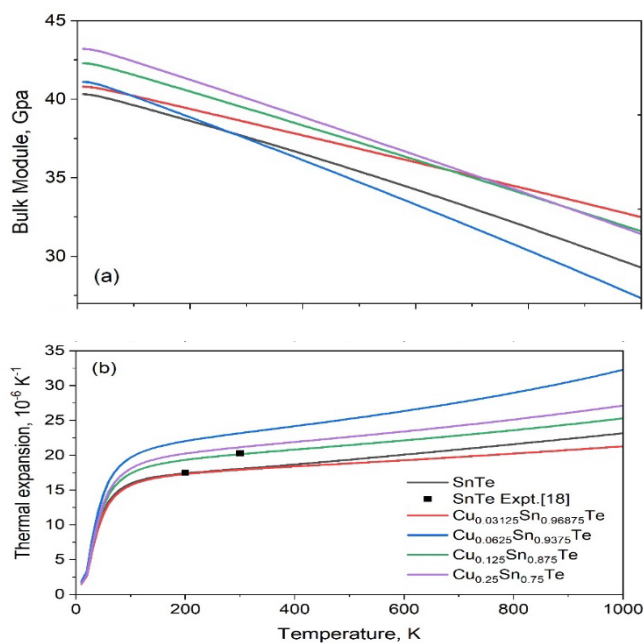
Fig. 7. Bulk modulus (a) and thermal expansion coefficients (b) of $Cu_xSn_{1-x}Te$ (x = 0, 0.03125, 0.0625, 0.125, 0.25) at finite temperatures, along with the available data measured by Nashchekina et al. [18].

Besides the slightly slower decline in modulus of $Cu_{0.03125}Sn_{0.96875}Te$, the decline rates of the moduli of the other compounds are similar and relatively fast. In the low-temperature area, the

thermal expansion coefficients of Cu doped SnTe compounds increases exponentially with temperature T, while it exhibits nearly linear behavior above 200 K, as demonstrated in Fig 7(b). For instance, at 200 K and 300 K, the present calculated thermal expansion coefficients of SnTe are 17.4×10^{-6} K^{-1} and 18.1×10^{-6} K^{-1}, which is in good accordance with the data of 17.5×10^{-6} K^{-1} at 200 K and 20.3×10^{-6} K^{-1} at 300 K measured by Nashchekina et al. [18].

4. Summary

First-principles calculations have been employed to examine the structural, electronic, mechanical, and thermodynamic characteristics of $Cu_xSn_{1-x}Te$ (x = 0, 0.03125, 0.0625, 0.125, 0.25) materials. The strain-stress method was utilized to determine mechanical properties, including B, G, E, and v. On the basis of the predicted elastic constants, the enthalpy of vacancy migration is also evaluated. The thermodynamic properties containing G, S, H, C_P, and C_V, together with the bulk modulus and thermal expansion coefficient varying with temperature are evaluated by the quasi-harmonic approach. All properties researched in current work are in excellent accordance with the existing measured results, calculated data or CALPHAD-modeled data. However, there is a lack of thermodynamic property of Cu doped SnTe materials, needing further research. For the $Cu_xSn_{1-x}Te$ (x = 0, 0.03125, 0.0625, 0.125, 0.25) compounds, the following conclusions are gained: (1) Through structural relaxation, all the materials studied in current work are stable in cubic phase. Furthermore, the $Cu_xSn_{1-x}Te$ (x = 0, 0.03125, 0.0625, 0.125, 0.25) compounds meet the stability criteria at all concentrations, with their enthalpy of formation satisfying the energy stability condition, and their elastic constants fulfilling the Born mechanical stability criterion. (2) With the exception of $Cu_{0.25}Sn_{0.75}Te$, as the proportion of Cu rises, B and v show an upward trend, whereas G and E exhibit a downward tendency. (3) $Cu_xSn_{1-x}Te$ (x = 0.03125, 0.0625, 0.125, 0.25) compounds all behave metallic. For SnTe, the bandgap evaluated by HSE06 is even close to the experimental data. With the increasing concentration of Cu, the influence of Cu-d electronic states on the bands near the Fermi level is increasing. (4) The thermodynamic properties of SnTe are in line with the CALPHAD results. In low temperature regions, the heat capacity increases sharply as the temperature rises. In the high temperature region, C_V approaches the Dulong-petit law. With the concentration of Cu increasing, the Debye temperature is increasing as well. The present calculated thermal expansion coefficients of SnTe at 200 K and 300 K are 17.4×10^{-6} K^{-1} and 18.1×10^{-6} K^{-1}, which agree well with the experimental data 17.5×10^{-6} K^{-1} and 20.3×10^{-6} K^{-1}.

References

[1] H.M. Yuan, J. Wang, B. Hu, R.Q. Zhao, Y. Du, S.Y. Zhang, Calphad, 68, 101743 (2020);
https://doi.org/10.1016/j.calphad.2020.101743

[2] W. Zhang, R. Mazzarello, M. Wuttig, E. Ma, Nat. Rev. Mater., 4, 150-168 (2019);
https://doi.org/10.1038/s41578-018-0076-x

[3] Z. Li, S. Li, J.P. Castellan, R. Heid, Y. Xiao, L.D. Zhao, Y. Chen, Y. Weber, Phys. Rev. B, 105, 014308 (2022); https://doi.org/10.1103/PhysRevB.105.014308

[4] L.D. Zhao, S.H. Lo, Y.S. Zhang, H. Sun, G.J. Tan, C. Uher, C. Wolverton, V.P. Dravid, M. G. Kanatzidis, Nature, 508, 373-377 (2014); https://doi.org/10.1038/nature13184

[5] K. Rajabi, E. Pakizeh, H. Tashakori, F. Taghizadeh-Farahmand, Solid State Commun., 359, 115023 (2023); https://doi.org/10.1016/j.ssc.2022.115023

[6] U.S. Shenoy, D.K. Bhat, Mater. Adv., 2, 6267–6271 (2021);
https://doi.org/10.1039/d1ma00696g

[7] A. Bugalia, V. Gupta, A. Pandey, J. Phys. D: Appl. Phys., 57, 195502 (2024);
https://doi.org/10.1088/1361-6463/ad2472

[8] J.F. Wang, N. Wang, H.Q. Huang, W.H. Duan, Chin. Phys. B, 25, 117313 (2016);
https://doi.org/10.1088/1674-1056/25/11/117313

[9] M. Muthumari, M. Manjula, K.Pradheepa, D.V. Kuznetsov, P. Veluswamy, J. Solid State Sci. Technol., 10, 071016 (2021); https://doi.org/10.1149/2162-8777/ac147c

[10] Z.L. Liu, Z.L. Guo, L. Deng, Inorg. Chem., 63(12), 5389-5399 (2024);
https://doi.org/10.1021/acs.inorgchem.3c03991

[11] M. Muthumari, M. Manjula, P. Veluswamy, D.V. Kuznetsov, J. Phys. Chem. Solids, 176, 111232 (2023); https://doi.org/10.1016/j.jpcs.2023.111232

[12] G. Jamwal, A. Kumar, M. Warish, S. Chakravarty, S. Muthiah,   A. Kandasami, A. Niazi, J. Alloys Compd., 954, 170182 (2023); https://doi.org/10.1016/j.jallcom.2023.170182

[13] L. Fu, C.L. Kane, Phys. Rev. B, 76, 045302 (2007);
https://doi.org/10.1103/PhysRevB.76.045302

[14] U. Paliwal, R.K. Kothari, K.B. Joshi, Superlattice Microst., 51, 635643 (2012);
https://doi.org/10.1016/j.spmi.2012.02.017

[15] A. Gueddim, N. Bouarissa, L. Gacem, A. Villesuzanne, Chin. J. Phys., 56, 1816-1825 (2018);
https://doi.org/10.1016/j.cjph.2018.08.014

[16] A. Gueddim, S. Zerroug, N. Bouarissa, N. Fakroun, Chin. J. Phys., 55, 1423-1431 (2017);
https://doi.org/10.1016/j.cjph.2017.04.009

[17] F.N. Guseinov, A.E. Seidzade, Y.A. Yusibov, M.B. Babanly, Inorg. Mater., 53, 4, 347-350 (2017); https://doi.org/10.1134/S0020168517040057

[18] O.N. Nashchekin, E.I. Rogachev, V.P. Popov, J. Phys. Chem. Solids, 69, 273-277 (2008);
https://doi.org/10.1016/j.jpcs.2007.07.019

[19] A.Z. Varisov, A.I. Rezanov, R.M. Sabitov, Izv. Vyssh. Uchebn. Zaved. Fiz., 5, 147-150 (1966);
https://doi.org/10.1007/BF00818192

[20] K.H. Timmesfeld, R.J. Elliot, Phys. Status Solidi, 42, 859-869 (1970);
https://doi.org/10.1002/pssb.19700420244

[21] V. Wang, N. Xu, J.C. Liu, G. Tang, W.T. Geng, Comput. Phys. Commun., 267, 108033 (2021); https://doi.org/10.1016/j.cpc.2021.108033

220

[22] W. Voigt, Annalen der Phys., 274, 573-587 (1889); https://doi.org/10.1002/andp.18892741206

[23] A. Reuss, Z. Angew. Math. Mech., 9(1) 49-58 (1929); https://doi.org/10.1002/zamm.19290090104

[24] S.L. Shang, Y. Wang, D.E. Kim, Z.-K. Liu, Comput. Mater. Sci., 47, 1040-1048 (2010); https://doi.org/10.1016/j.commatsci.2009.12.006

[25] O.L. Anderson, Oxford University Press, New York, (1995);

[26] V.L. Moruzzi, J.F. Janak, K. Schwarz, Phys. Rev. B, 37, 790-799 (1988); https://doi.org/10.1103/PhysRevB.37.790

[27] G. Kresse, J. Furthmuller, Phys. Rev. B, 54, 11169-11186 (1996); https://doi.org/10.1103/PhysRevB.54.11169

[28] G. Kresse, J. Furthmuller, Comput. Mater. Sci., 6, 11-50 (1996); https://doi.org/10.1016/0927-0256(96)00008-0

[29] G. Kresse, D. Joubert, Phys. Rev. B, 59, 1758-1775 (1999); https://doi.org/10.1103/PhysRevB.59.1758

[30] J.P. Perdew, K. Burke, M. Ernzerhof, Phys. Rev. Lett., 77, 3865-3868 (1996); https://doi.org/10.1103/PhysRevLett.77.3865

[31] J. Heyd, G.E. Scuseria, M. Ernzerhof, J. Chem. Phys., 118, 8207-8215 (2003); https://doi.org/10.1063/1.1564060

[32] M. Methfessel, A.T. Paxton, Phys. Rev. B, 40, 3616-3621 (1989); https://doi.org/10.1103/PhysRevB.40.3616

[33] P.E. Blöchl, O. Jepsen, O.K. Andersen, Phys. Rev. B, 49, 16223-16233 (1994); https://doi.org/10.1103/PhysRevB.49.16223

[34] H.J. Monkhorst, J.D. Pack, Phys. Rev. B, 13, 5188-5192 (1976); https://doi.org/10.1103/PhysRevB.13.5188

[35] R.J. Cava, H. Ji, M.K. Fuccillo, Q.D. Gibson, Y.S. Hor, J. Mater. Chem. C, 1, 3176-3189 (2013); https://doi.org/10.1039/C3TC30186A

[36] O. Madelung, Springer, Berlin, (2004); https://doi.org/10.1007/978-3-642-18865-7

[37] P.B. Pereira, I. Sergueev, S. Gorsse, J. Dadda, E. Muller, R.P. Hermann, Phys. Stat. Sol. B, 250, 1300–1307 (2013); https://doi.org/10.1002/pssb.201248412

[38] J. Kumar, P. Tanwar, U. Paliwal, K. B. Joshi, J. Mol. Model., 29, 335 (2023); https://doi.org/10.1007/s00894-023-05742-x

[39] C M I Okoye, J. Phys.: Condens. Matter, 14, 8625 (2002); https://doi.org/10.1088/0953-8984/14/36/318

[40] N.E. Zein, V.I. Zinenko, A.S. Fedorov, Phys. Lett. A, 164, 115-119 (1992); https://doi.org/10.1016/0375-9601(92)90916-A

[41] K. Lejaeghere, V. VanSpeybroeck, G.V. Oost, S. Cottenier, Crit. Rev. Solid State Mater. Sci., 39, 1-24 (2014); https://doi.org/10.1080/10408436.2013.772503

[42] G. Murtaza, K. Ismail, S. Tahir, J. Solid State Chem., 314, 123432 (2022); https://doi.org/10.1016/j.jssc.2022.123432

[43] A.G. Every, A.K. McCurdy, Springer-Verlag, Berlin, 29, (1992); https://doi.org/10.1007/b44185

[44] F. Mouhat, F.X. Coudert, Phys. Rev. B, 90, 224104 (2014); https://doi.org/10.1103/PhysRevB.90.224104

[45] S. Chattopadhyaya, U. Sarkar, B. Debnath, M. Debbarma, D. Ghosh, S. Chanda, R.

Bhattacharjee, Comput. Condens. Matter, 20, e00384 (2019);
https://doi.org/10.1016/j.cocom.2019.e00384

[46] H. Siethoff, Intermetallics 5, 625-632 (1997); https://doi.org/10.1016/S0966-9795(97)00037-X

[47] T. Angsten, T. Mayeshiba, H. Wu, D. Morgan, New J. Phys., 16, 015018 (2014);
https://doi.org/10.1088/1367-2630/16/1/015018

[48] M. Markov, X. Hu, H.C. Liu, N. Liu, S.J. Poon, K. Esfarjani, M. Zebarjadi, Sci. Rep., 8(1), 1-10 (2018); https://doi.org/10.1038/s41598-018-28043-3

[49] R.M. Kannaujiya, A.J. Khimani, S.H. Chaki, S.M. Chauhan, A.B. Hirpara, M.P. Deshpande, Eur. Phys. J. Plus, 135, 47 (2020); https://doi.org/10.1140/epjp/s13360-019-00022-1

[50] X.J. Tan, H.Z. Shao, J. He, G.Q. Liu, J.T. Xu, J. Jiang, H.C. Jiang, Phys. Chem. Chem. Phys., 18, 7141-7147 (2016); https://doi.org/10.1039/C5CP07620J

[51] N. Wang, D. West, J. Liu, J. Li, Q. Yan, B.L. Gu, S.B. Zhang, W.H. Duan, Phys. Rev. B, 89, 045142 (2014); https://doi.org/10.1103/PhysRevB.89.045142

[52] R. Moshwan, W.D. Liu, X.L. Shi, Y.P. Wang, J. Zou, Z.C. Chen, Nano Energy, 65, 104056 (2019); https://doi.org/10.1016/j.nanoen.2019.104056

[53] K.B. Joshi, U. Paliwal, B.K. Sharma, Phys. Status Solidi B, 248, 1248-1252 (2011);
https://doi.org/10.1002/pssb.201046332

[54] Y.J. Liu, D. Liang, L.J. Zhang, J. Electron. Mater., 39(2), 246-257 (2010);
https://doi.org/10.1007/s11664-009-0985-y

[55] A.T. Petit, P.L. Dulong, Ann. Chim. Phys., 1819, (1819);
https://web.lemoyne.edu/~giunta/petit.html